PROCEEDINGS OF SCIENCE

ONLINE ICRC 2021
THE ASTROPARTICLE PHYSICS CONFERENCE
Berlin | Germany
37th International Cosmic Ray Conference
12–23 July 2021

Multiwavelength observations in 2019–2020 of a new very-high-energy γ-ray emitter: the flat spectrum radio quasar QSO B1420+326

Filippo D'Ammando,[a,*] **Roberto Angioni,**[b] **Monica Orienti,**[a] **on behalf of the Fermi Large Area Telescope Collaboration, Julian Sitarek,**[c] **Seiya Nozaki,**[d] **Elina Lindfors,**[e] **Giacomo Bonnoli,**[f] **Vandad Fallah Ramazani,**[e,g] **on behalf of the MAGIC Collaboration and Svetlana Jorstad**[h]

[a] *INAF-IRA Bologna, Via P. Gobetti 101, I-40129 Bologna, Italy*

[b] *ASI Space Science Data Center, Via del Politecnico snc., I-00133 Rome, Italy*

[c] *University of Lodz, Faculty of Physics and Applied Informatics, Department of Astrophysics, Pomorska 149, P-90-236 Lodz, Poland*

[d] *Department of Physics, Kyoto University, Kitashirakawa-Oiwakecho, Sayko-ku, 606-8502 Kyoto, Japan*

[e] *Finnish Centre for Astronomy with ESO, University of Turku, Quantum, Vesilinnantie 5, FI-20014 Turku, Finland*

[f] *Instituto de Astrofisica de Andalucia, Glorieta de la Astronomia, s/n, S-18008 Granada, Spain*

[g] *Ruhr University Bochum, Universitätsstraße 150, D-44801 Bochum, Germany*

[h] *Institute for Astrophysical Research, Boston University, 725 Commonwealth Avenue, Boston, MA 02215, United States*

E-mail: dammando@ira.inaf.it

*Presenter

PoS(ICRC2021)775

The flat-spectrum radio quasar QSO B1420+326 underwent an enhanced γ-ray flux state seen by *Fermi*-LAT at the turn of 2019/2020. Compared to the low state both the position and luminosity of the two spectral energy distribution peaks changed by at least two orders of magnitude. The high state resulted in the discovery of the very-high-energy (>100 GeV) γ-ray emission from the source by the MAGIC telescopes. The organized multiwavelength campaign allow us to trace the broadband emission of the source through different phases of the flaring activity. The source was observed by 20 instruments in radio, near-infrared, optical, ultra-violet, X-ray and γ-ray bands. We use dedicated optical spectroscopy results to estimate the accretion disc and the dust torus luminosity. The optical spectroscopy shows a prominent FeII bump with flux evolving together with the continuum emission and a MgII line with varying equivalent width. The γ-ray flare was accompanied by a rotation of the optical polarization vector and emission of a new superluminal radio knot. We model spectral energy distributions in different flare phases in the framework of combined synchrotron-self-Compton and external Compton scenario in which the shape of the electron energy distribution is determined from cooling processes.

37th International Cosmic Ray Conference (ICRC 2021)
July 12th – 23rd, 2021
Online – Berlin, Germany

1. Introduction

The population of blazars represents a sub-class of active galactic nuclei (AGN) dominating the extragalactic γ-ray sky whose jet axis is closely aligned with our line of sight. The jet emission of blazars is highly amplified due to Doppler boosting effects, and a high level of variability is detected at all wavelengths. Blazars are traditionally divided into flat spectrum radio quasars (FSRQ) and BL Lac objects (BL Lacs), based on the presence or not, respectively, of broad emission lines (i.e., equivalent width > 5 Å) in their optical and UV spectrum [e.g., 16]. This is related to a different accretion regime that reflects on an additional external source of seed photons for inverse Compton (IC) scattering in FSRQ, leading to the observed Compton peak dominance in FSRQ with respect to BL Lacs [e.g., 9]. FSRQ constitute a small subgroup of AGN detected in very-high-energy (VHE; E > 100 GeV) γ-rays (only 8 detected up to now[1]). Although FSRQ are generally brighter than BL Lacs, their IC bumps peak at lower energies, resulting in softer VHE spectra. In addition, they are mostly located at higher redshifts, with their VHE spectra further softened by absorption on the extragalactic background light (EBL; see, e.g., 6), hampering the discovery potential in this energy range. Moreover, if the emitting region lies within the Broad Line Region (BLR) the VHE emission from FSRQ is expected to be absorbed internally by the photons emitted by the accretion disc and reprocessed by the BLR for γ-γ absorption. Finally, FSRQ are known to be extremely variable (see, e.g., 11), which is another issue in discovering those sources with instruments with relatively small fields of view such as Imaging Atmospheric Cherenkov Telescopes. Considering the lack of information about FSRQ detected at VHE, dense follow-up observations of new FSRQ detected at VHE are fundamental.

QSO B1420+326, also known as OQ 334, is a FSRQ located at redshift z = 0.682 [10]. Following a high activity period observed at high-energy (HE; 100 MeV < E < 100 GeV) γ-rays by the Large Area Telescope (LAT) on board the *Fermi Gamma-ray Space Telescope* lasting for a few weeks [3], the MAGIC collaboration has reported in 2020 January the first detection of VHE γ-ray emission from this source [13]. QSO B1420+326 is the fourth most distant VHE γ-ray source known to date. Due to the duration of the enhanced state, several observatories were alerted and were able to follow the development of the flare from radio up to VHE γ-rays [e.g., 4, 7, 12], including Very Long Baseline Array (VLBA) observations.

In this paper, we report on the most interesting results on the broadband observations of QSO B1420+326 triggered by the 2019/2020 high state and other contemporaneous multiwavelength (MWL) data, summarizing the results presented in Acciari et al. [2]. The results of the observations are reported in Section 2. In Section 3, we model the broadband emission of the source in different phases of the high state, while conclusions are drawn in Section 4. We use cosmological parameters H_0 = 67.4 km/s/Mpc, Ω_Λ = 0.6847, and Ω_M = 0.315 [15].

2. MWL light curves

In Fig. 1 we present the multiwavelength light curves of the source collected from VHE γ-rays to radio between 2019 December 28 (MJD 58845) and 2020 February 11 (MJD 58890). Detailed descriptions of the instruments involved in the campaign, the data taken and the analysis methods are

[1] see http://tevcat.uchicago.edu/

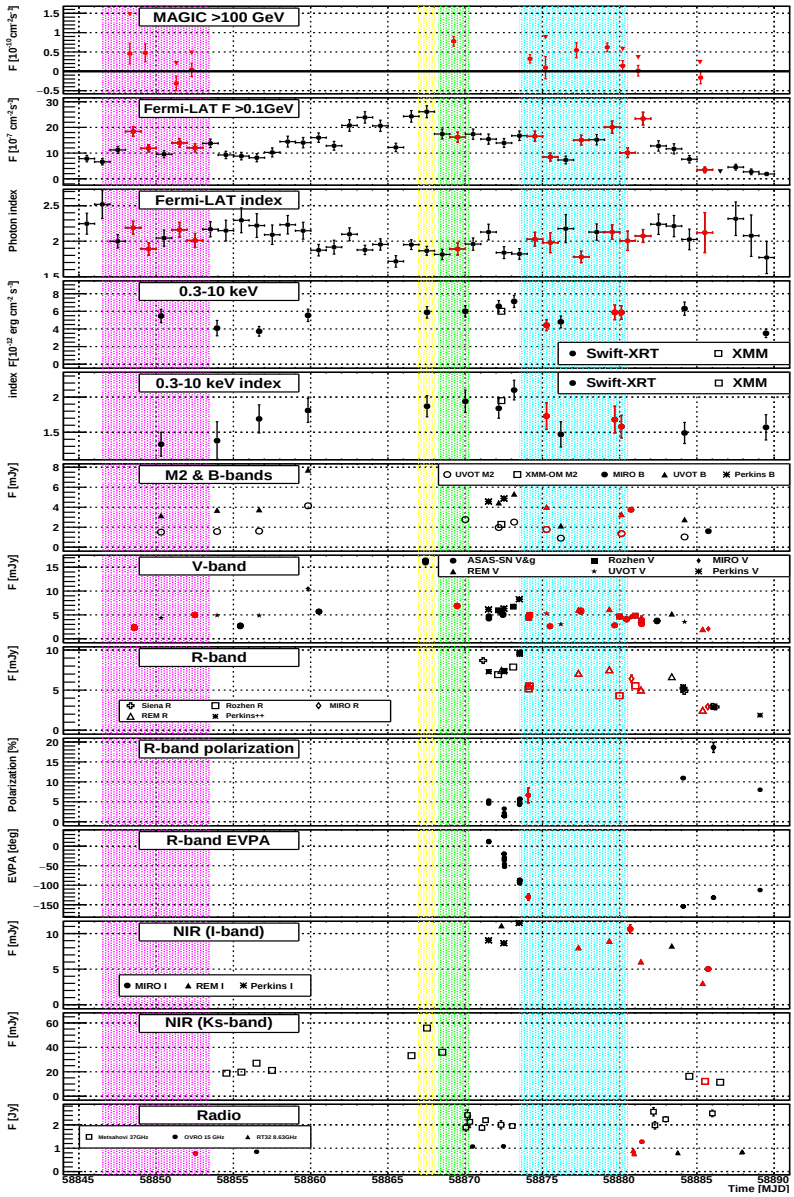

Figure 1: MWL light curve of QSO B1420+326 between 2019 December 28 (MJD 58845) and 2020 February 11 (MJD 58890). Optical and UV observations are corrected for the Galactic extinction. Red points are contemporaneous (±12 hr) with MAGIC observations. The shaded regions show the time ranges of the four periods (see Table 1) used for the SED modeling. Flux upper limits in the first two panels are shown with downward triangles. Figure reproduced from Acciari et al. [2].

Period	MJD	Activity State
A	58846.5 - 58853.5	pre-flare
B	58867 - 58868	optical flare
C	58868.3 - 58870.3	VHE flare
D	58873.5 - 58880.5	post-flare

Table 1: Periods selected for the SED modeling. Colors are the same used in Figs. 1 and 2.

reported in [2]. We define four periods (A–D) based on the VHE state of the source, as summarized in Table 1. In case of period B, no simultaneous MAGIC data are available but the period refers to the peak of the optical and infrared flare as well as one of the local peaks of HE emission.

The first detection of the source at VHE by MAGIC was obtained on 2020 January 20 (MJD 58868), at 14.3-σ in 1.6 hr of effective time. Further hints of signal are obtained during 2020 January 26–February 1 (MJD 58874–58880), with the highest significance of the excess (6.6-σ) on 2020 January 31 (MJD 58879), corresponding to the longest exposure of 2.5 hr. During the VHE flare (period C), the flux reached $(7.8 \pm 1.3_{\rm stat}) \times 10^{-11}$ cm^{-2} s^{-1}. The observed spectrum in this period can be described by a power-law: $dN/dE = (2.49 \pm 0.31_{\rm stat}) \times 10^{-9}\,(E/100\,{\rm GeV})^{-4.22\pm0.24_{\rm stat}}$ [TeV^{-1} cm^{-2} s^{-1}]. Correcting for the EBL absorption according to [6], the unattenuated spectrum can be described as: $dN/dE\, e^{\tau_{\rm EBL}(E)} = (4.04 \pm 0.54_{\rm stat}) \times 10^{-9}\,(E/100\,{\rm GeV})^{-3.57\pm0.29_{\rm stat}}$ [TeV^{-1} cm^{-2} s^{-1}]. After the flare (period D), significant (5.6-σ) emission is detected again, but at a flux about half the flare level, $(3.9 \pm 0.6_{\rm stat})\times10^{-11}$ cm^{-2} s^{-1} with a spectrum corrected for EBL absorption $dN/dE\, e^{\tau_{\rm EBL}(E)} = (1.64 \pm 0.22_{\rm stat}) \times 10^{-9}\,(E/100\,{\rm GeV})^{-2.87\pm0.36_{\rm stat}}$ [TeV^{-1} cm^{-2} s^{-1}]. The spectral indices during and after the flare are consistent within 1.5-σ. Before the flare (period A), no significant emission is detected, possibly due to shorter observations under less favorable zenith angle. The corresponding upper limit (95% C.L.) is $< 4.1 \times 10^{-11}$ cm^{-2} s^{-1}, comparable to the flux detected in period D.

Both the flux and the photon index observed by *Fermi*-LAT on daily basis were significantly variable. The maximum HE flux was observed on 2020 January 19 (MJD 58867), $(2.6 \pm 0.2) \times 10^{-6}$ cm^{-2} s^{-1}, corresponding to about 300 times the average flux reported in the fourth Fermi LAT catalog [4FGL; 1]. The highest-energy photon was observed by the LAT on 2020 January 17 (MJD 58865), with an energy of ~150 GeV. The hardest photon index was detected on the same date ($\Gamma_{\rm HE}$ = 1.72 ± 0.08). More generally, the photon index was consistently harder than the 4FGL catalog value ($\Gamma_{\rm 4FGL}$ = 2.38 ± 0.07) during most of the period studied.

No strong flux variability was observed in X-rays, with an increasing trend from 2020 January 5 (MJD 58853) to 2020 January 25 (MJD 58873), where a peak flux a factor of 2 higher is detected. On the other hand, a harder-when-brighter behaviour has been observed by *Swift*-XRT over the period, suggesting a shift of the synchrotron peak to higher energies. Thus is reflected in a shift of the crossing point between the synchrotron and IC component, clearly visible in the *XMM-Newton* spectrum collected on 2020 January 24.

A strong optical flare was observed on 2020 January 19 (MJD 58867; Period B) with a variability time scale of the order of a few days, and an increase by an order of magnitude with respect to the observations performed at the beginning of Period A. Similar variability pattern is seen also in IR and UV ranges, although the IR-UV spectrum becomes harder (bluer) during the optical flare, in agreement with a shift of the synchrotron peak position inferred from X-ray observations. Optical polarizations showed a dip of the polarization percentage at a few per cent level and a concurrent rotation by ~150° after the VHE flare. The optical spectroscopy observations performed by the Lowell Discovery Telescope on 2020 January 28, February 8 and 25 revealed a prominent MgII line, that does not show flux variability exceeding the uncertainties of the measurements, in agreement with a production within a canonical BLR. Using the MgII line as a proxy for estimating the accretion disc luminosity, we obtained $L_{\rm d} = 2 \times 10^{46}$ erg s^{-1}. We observed also a significant decrease of the equivalent width as the continuum rises. A broad FeII bump has been observed

Period	$\delta = \Gamma$	r_b [cm]	ξ	B [G]	U'_e [10^{48}erg]	p_1	$\gamma_{\rm min}$	p_2	$\gamma_{\rm break}$	$\gamma_{\rm max}$	u'_e [erg cm^{-3}]	u'_e/u'_B
A	40	6.16×10^{16}	0.3×10^{-7}	0.70	1.18	1.7	1	2.7	63	6900	1.2×10^{-3}	0.06
B	40	3.70×10^{16}	0.3×10^{-7}	0.95	1.76	1.8	15	2.8	104	8000	8.3×10^{-3}	0.23
C	40	3.08×10^{16}	3.0×10^{-7}	0.83	2.12	2.0	10	3.0	125	23700	17.3×10^{-3}	0.63
D	40	3.08×10^{16}	6.0×10^{-7}	0.55	2.35	2.0	10	3.0	125	27300	19.2×10^{-3}	1.6

Table 2: Parameters used for the modeling: Doppler factor δ ($\Gamma = \delta$ is assumed), co-moving size of the emission region r_b, acceleration parameter ξ, magnetic field B, total energy of electron U'_e, electron energy distribution: slope before the break p_1, minimum Lorentz factor $\gamma_{\rm min}$, slope after the break p_2, the Lorentz factor of the break $\gamma_{\rm break}$, maximum Lorentz factor $\gamma_{\rm max}$, electron energy density u'_e, energy equipartition u'_e/u'_B. Free parameters of the model and derived parameters are put on the left and right side of the double vertical line respectively

increasing in flux contemporaneously to the synchrotron continuum level, suggesting an origin in a much smaller region than the BLR, likely located close to the jet axis. The behaviour shown by optical spectroscopy could be related to an interaction between the non-thermal jet emission with an FeII-emitting cloud, while the MgII emission is excited by the underlying thermal accretion disc continuum, which varies on a much longer time scale.

Moderate variability was observed in radio observations. In particular, OVRO data at 15 GHz showed a gradual increase of the flux. In addition, high-resolution VLBA observations at 43 GHz pinpointed the ejection of a superluminal radio knot (K20) contemporaneous with the high γ-ray state with an apparent speed of $\beta_{\rm app} = 12.0 \pm 1.7$ and the passage of K20 through the VLBA core on MJD 58831 ± 21 (2019 December 13).

3. SED modeling

We modeled the source in a framework of a simple one-zone model in which a spherical emission region is homogeneously and isotropically filled with an electron distribution and magnetic field. The γ-ray emission from FSRQ is usually explained in the framework of an external Compton (EC) model. Since the source emits up to VHE range, the most natural target seed photons for the EC process is the dust torus (DT) radiation field that does not absorb strongly the sub-TeV γ-rays. On the other hand, the large increase of the optical flux at the time of the γ-ray flare can provide a significant seed source for synchrotron-self-Compton (SSC) process. Both scenarios are investigated by the SED modeling of the four periods A–D (see Fig. 2). The SED model was generated with `agnpy`[2] [14], which implements the synchrotron and Compton processes following the prescriptions described in [5, 8]. We fix the Lorentz and Doppler factors of the blob to $\Gamma = 40$ and $\delta = 40$, respectively. The size of the blob is limited by the variability condition. We consider a broken power-law energy distribution of electrons. More details are reported in Acciari et al. [2]. All parameters for the four SED are reported in Table 2. A satisfactory description of the SED can be obtained by the combination of synchrotron and EC(DT) processes, similarly to other FSRQ detected at VHE. The variability of the emission between different phases of the enhanced state is explained mainly by a combination of variations of the compactness of the emitting region, the minimal injection energy of electrons and increase of the acceleration parameters. In addition

[2]https://github.com/cosimoNigro/agnpy/

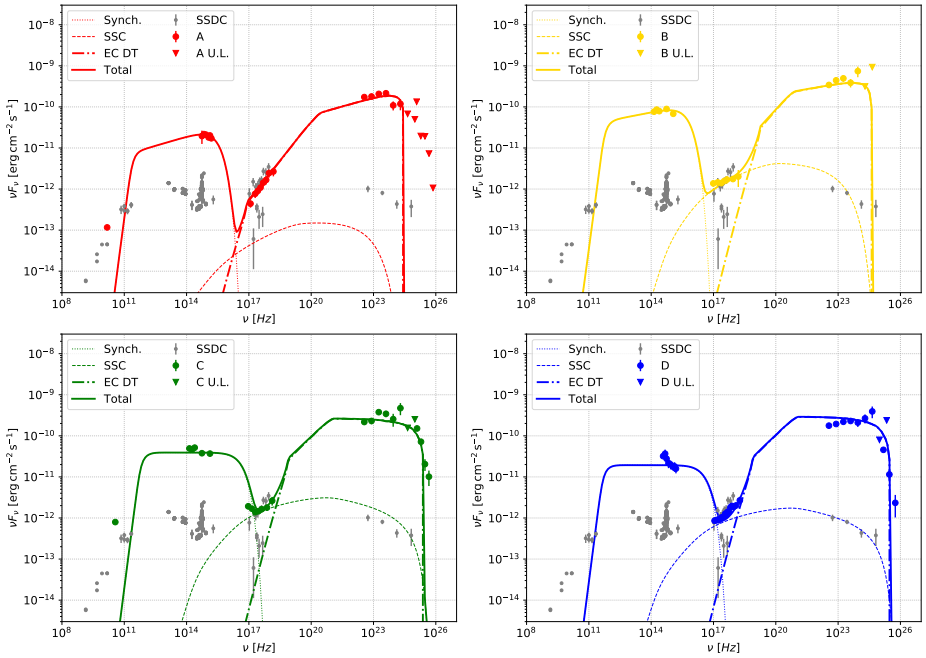

Figure 2: Multiwavelength SED of the source in the four periods: A – before the flare, B – optical flare, C – VHE γ-ray flare, D – after the flare. Archival data are shown in gray. Different radiation processes are shown with different line styles: dotted lines – synchrotron, dashed – SSC, dot-dashed – EC, solid – sum of components. Model lines are corrected for EBL absorption according to Domínguez et al. [6]. Figure reproduced from Acciari et al. [2].

small variations of the magnetic field, total energy stored in electrons, and injection slope has been assumed.

4. Conclusions

The observations of QSO B1420+326 with the MAGIC telescopes during a high γ-ray activity period detected by *Fermi*-LAT resulted in adding this source to the rare family of VHE-detected FSRQ. Thanks to the extensive MWL monitoring campaign organized in 2020 January–February, which allowed us to track and model the evolution of the broadband emission, the detection at VHE of QSO B1420+326 has provided a new piece to solving the puzzle of the origin of the highest energy emission of FSRQ. Similarly to other VHE-detected FSRQ, the ejection of a new radio knot and the rotation of optical electric vector position angle (EVPA) were detected close in time to the VHE emission. The spectra in different periods (from pre-flare to post-flare passing through the VHE flare) are Compton dominated, which is typical for FSRQ, but the dominance during the peak of the flare is just a factor of a few. The SED at different epochs around the VHE detection is well explained in the EC(DT) scenario with electron energy distribution limited by an interplay of acceleration, dynamic and cooling time scales.

Acknowledgments

MAGIC Collaboration: We would like to thank all the institutions and agencies listed here: https://magic.mpp.mpg.de/ack-202009/.

Fermi-LAT Collaboration: The *Fermi*-LAT Collaboration acknowledges support for LAT development, operation and data analysis from NASA and DOE (United States), CEA/Irfu and IN2P3/CNRS (France), ASI and INFN (Italy), MEXT, KEK, and JAXA (Japan), and the K.A. Wallenberg Foundation, the Swedish Research Council and the National Space Board (Sweden). Science analysis support in the operations phase from INAF (Italy) and CNES (France) is also gratefully acknowledged. This work performed in part under DOE Contract DE-AC02-76SF00515.

References

[1] Abdollahi, S., et al 2020, ApJS, 247, 33

[2] Acciari, V. A., et al. 2021, A&A, 647, A163

[3] Ciprini, S., Cheung, C. C. 2020, The Astronomer's Telegram 13382

[4] D'Ammando, F., Fugazza, D., Covino, S. 2020, The Astronomer's Telegram 13428

[5] Dermer, C. D. & Menon, G. 2009, High Energy Radiation from Black Holes: Gamma Rays, Cosmic Rays, and Neutrinos by Charles D. Dermer and Govind Menon. Princeton Univerisity Press, November 2009

[6] Domínguez, A., et al. 2011, MNRAS, 410, 2556

[7] Fallah Ramazani, V., Bonnoli, G., D'Ammando, F., Cerruti, M., Righi, C., Sitarek, J. 2020, The Astronomers' Telegram 13417

[8] Finke, J. D. 2016, ApJ, 830, 94

[9] Ghisellini, G., Righi, C., Costamante, L., Tavecchio, F. 2017, MNRAS, 469, 225

[10] Hewett, P. C., & Wild, V. 2010, MNRAS, 405, 2302

[11] Meyer, M., Scargle, J. D., & Blandford, R. D. 2019, ApJ, 877, 39

[12] Minev, M., Kurtenkv, A., Ovcharov, E. 2020, The Astronomer's Telegram 13421

[13] Mirzoyan, R. 2020, The Astronomer's Telegram 13412

[14] Nigro, C., Sitarek, J., Craig M. & Gliwny, P. 2020, agnpy: modeling Active Galactic Nuclei radiative processes with python. Zenodo. http://doi.org/10.5281/zenodo.4055176

[15] Planck Collaboration, Aghanim, N., et al. 2020, A&A, 641, A6

[16] Stickel M., Padovani, P., Urry, C. M., Fried, J. W., Kuehr, H. 1991, ApJ, 374, 431